

# Gypsum board failure model based on cardboard behaviour

D. Lázaro<sup>1</sup>, E. Puente<sup>1</sup>, J. Peña<sup>2</sup>, D. Alvear<sup>1</sup>

<sup>1</sup>GIDAI, University of Cantabria, Avda. Los Castros, s/n, 39005 Santander. SPAIN

<sup>2</sup>GRUPO URALITA, División Yesos Ibéricos, Ctra de Andalucía Km. 30,200, 28340 Madrid SPAIN

## ABSTRACT

This study aims to analyse the importance of gypsum plasterboard cardboard for fire resistance. A new hypothesis considering the failure based on the cardboard degradation is defined. This hypothesis comes from the thermal analysis of gypsum and cardboard performed in the simultaneous thermal analysis apparatus (STA). STA results also allow defining the dehydration process of the gypsum. A numerical model that considers gypsum dehydration and the failure hypothesis has been developed using Fire Dynamic Simulator. This numerical model is validated against six fire resistance tests. Results show that we can appropriately tune the numerical model (for predicting time to failure) based on the thermal properties of cardboard.

**KEYWORDS:** heat transfer, compartment fires, fire modelling, fire resistance tests, gypsum plasterboard, thermogravimetric analysis.

## 1. INTRODUCTION

Fire resistance of building systems is a critical aspect of building safety design. One of the most used passive fire protection elements is gypsum plasterboard. These plasterboards can be designed with different characteristics according to the desired use and specifically the best fire resistance properties are provided by type F gypsum plasterboard, which has fibres in the core that increase its resistance to fall out during fires.

Nowadays, it is also important to increase the energy efficiency of buildings and ensure comfortable conditions therein. This implies that, in a large number of cases, insulation materials should be included in the system. Although there are several sorts of insulation materials, mineral wool provides good thermal insulation and fire resistance performances [1].

The European normative standards EN 1363 and EN 1364 [2-4] established the requirements to perform fire resistance tests for non-load-bearing elements, walls, and ceilings. The criterion for failure, as defined by the standards, are that the average temperature in the unexposed face exceeds 140 °C above the initial temperature or the temperature of the unexposed face at any point increases to more than 180 °C above the initial temperature. Those temperatures can be reached directly by heat transfer through the whole system or by a part of the system if the thermal attack causes a deflection that, in turn, provoke boards to fall out [5].

Several models found reasonably good agreement with the experimental data when focusing on the heat transfer process without considering the ablation and fall off effect [6, 7, 8]. Hopkin et al. [6] used the finite element software DIANA [9] to simulate the heat transfer over Structural Insulated Panels and Engineered Floor Joists that contains gypsum plasterboards. This system was fixed on vertical timber battens. Keerthan et al. [10] used SAFIR [11] to model the thermal behaviour of gypsum plasterboard panels of dimensions 1350 mm x 1080 mm. This size increases the inertia of the system, avoiding the mechanical forces effect in the experiment and in the model. Kolaitis et al. [8] included in its FDS model

the quantification of the water vapour released from the gypsum plasterboards due to gypsum dehydration. This model has been validated versus two pairs of commercially available 12.5 mm thick gypsum plasterboard, measuring 1250 mm x 1050 mm, separated by a 75mm U-shaped steel stud. The size of the system avoids mechanical effect in the experimental test. Thanasoulas et al. [12] combine two different kind of models to add the thermal effect on the structure of the system. Firstly, they used ANSYS CFX [13] to develop a transient heat transfer model that provide the spatial and temporal temperature variation over a drywall assembly. Then, the thermal simulation results were introduced in a subsequent structural analysis performed with ADINA [14]. The influence in the fire resistance tests of the cardboard contained in the gypsum plasterboards is not studied in the literature, nor the plasterboard fall off due to the temperature.

In our previous work [15], the ablation in the model for the exposed boards of partition systems was studied. We hypothesized that this may well occur at the temperature of the endothermic reaction in the gypsum that correlates to a transition between a material that is easy to rehydrate by forming hemihydrates and another material that is difficult to rehydrate by absorbing water. The effect of the cardboard in the fire resistance of the gypsum plasterboard systems was not studied either.

When different tests were developed, we could observe that the cardboard fire behaviour is not likely negligible. Therefore, in the present paper, a new hypothesis considering the failure based on the cardboard degradation was defined. We analysed different kinds of gypsum and the cardboard used to cover the type F gypsum plasterboard with thermal analysis tests and six standard fire tests. We also incorporate to the model the possibility of simulate a system with mineral wool for insulation. In the end, the model was validated with the standard fire tests.

The paper is organized as follows. Section 2 presents the STA results, which will support assumption in the model. Section 3 describes the standard fire tests of gypsum plasterboard systems. Section 4 explains the thermal model and evaluates its results comparing them with the standard fire tests. Section 5 concludes the paper.

## 2. SMALL-SCALE TESTS

An initial thermal characterization was performed for the plasterboards used in the fire resistance tests. We used simultaneous thermal analysis (STA) (Netzsch STA 449 F3), which allows us to determine the typical temperatures at which the processes take place, the mass loss in each process by thermal gravimetric (TG) analysis and the heat of reaction by differential scanning calorimetry (DSC). These results were the key parameters used in the computational model. Table 1 shows the description of the materials tested and the conditions of the tests. Two kinds of gypsum plasterboards are tested. Standard gypsum plasterboard (type N gypsum plasterboard) is classified as type A in EN 520:2004+A1:2009, and a fire protection gypsum plasterboard (type F gypsum plasterboard) is classified as type F in EN 520:2004+A1:2009. Type F gypsum plasterboard contains mineral fibres in the gypsum core to enhance its cohesion at high temperatures. The heating rate used in every test was 10 K·min<sup>-1</sup>. We chose this heating rate because of it is widely used in literature [16].

Figure 1 displays STA curves for a sample of 18.689 mg of type N gypsum plasterboard. The density of this type N gypsum plasterboard was 691 kg·m<sup>-3</sup>.

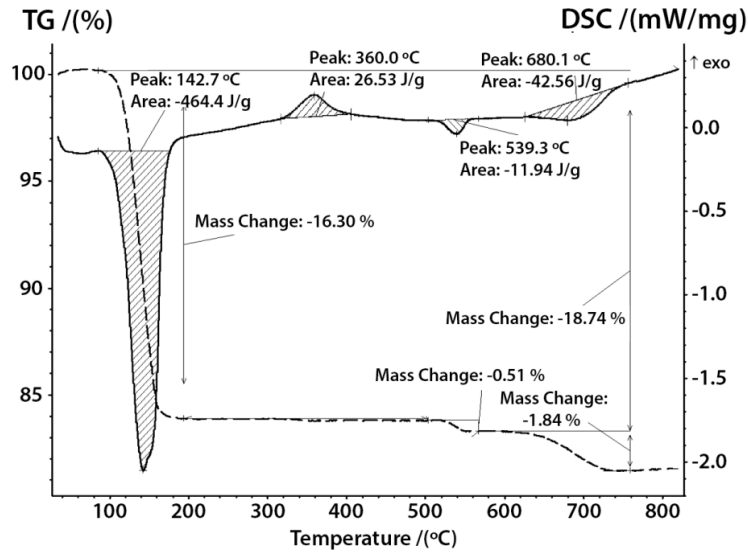


Fig. 1. DSC (solid line) and TG (dashed line) results for type N gypsum plasterboard.

Table 2 shows the results extracted from the data in Figure 1 where five different processes that occur in the gypsum can be observed. The first and second are the endothermic reactions corresponding to the dehydration reactions that occur between 90 and 194 °C with the peak at 142 °C. The heat absorbed during dehydration is approximately  $464.4 \text{ J}\cdot\text{g}^{-1}$ . The gypsum loses 16.30 % of its water mass content. Both dehydration reactions are temperature-overlapped, and they are defined by the chemical reaction equations (1) and (2).



The next reaction takes place between 332.5 and 383.9 °C and corresponds to the transition in the crystalline structure of gypsum from the soluble to the insoluble anhydride  $\text{CaCO}_4$ . This transition reaction is exothermic and releases a heat of reaction of approximately  $26.53 \text{ J}\cdot\text{g}^{-1}$ . The chemical reaction of this process is defined in (3).



Where Q is the energy released.

The two remaining processes are associated with the type and amount of impurities and additives in the gypsum. The next reaction is endothermic and has its peak at 539.3 °C and a heat of reaction of approximately  $11.94 \text{ J}\cdot\text{g}^{-1}$ . The final endothermic reaction absorbs a total amount of heat of approximately  $42.56 \text{ J}\cdot\text{g}^{-1}$  and occurs at 680.1 °C (peak temperature).

STA results for a sample of 15.3 mg of the type F gypsum plasterboard are shown in Figure 2. This sort of gypsum plasterboard has a higher quantity of glass fibre that improves the fire behaviour of the gypsum. The density of the type F gypsum plasterboard was  $777 \text{ kg}\cdot\text{m}^{-3}$ .

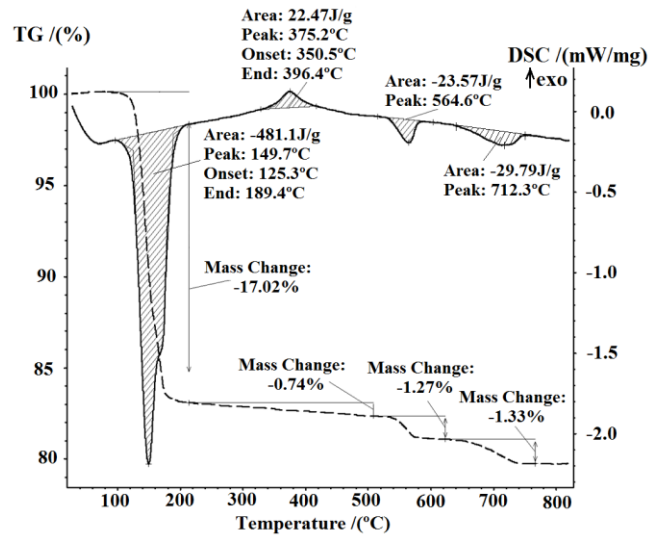


Fig. 2. DSC (solid line) and TG (dashed line) results for type F gypsum plasterboard.

It can be seen in Table 3 the results extracted from those data. Although one observes the same five processes that type N gypsum plasterboard undergoes, they have some differences. Firstly, the endothermic dehydration reaction occurs between 125.3 and 189.4 °C with the peak at 149.7 °C. The heat absorbed during dehydration is 481.1 J·g<sup>-1</sup>. This gypsum loses 17.02 % of its water. The transition in the crystalline structure occurs between 350.5 and 396.4 °C, where we express the transition temperature as a range and not as a single temperature since it depends on both the sample homogenization and the heat distribution in the sample and impurities in the sample may change this value. This transition reaction is exothermic and releases a heat of reaction of approximately 22.47 J·g<sup>-1</sup>, which closely approximates the heat value released by the type N gypsum plasterboard, even though it occurs at higher temperatures in type F gypsum plasterboard. The next reaction occurs at 564.6 °C, which is also nearly that found for the type N gypsum plasterboard. However, the heat of reaction is 23.57 J·g<sup>-1</sup>, which is more than three times higher in this case. The last endothermic reaction absorbs a total amount of heat of 29.79 J·g<sup>-1</sup>, close to six times lower than that of the type N gypsum plasterboard, despite the fact that the peak temperature is 717.5 °C, which approaches to the previous gypsum plasterboard.

The main property of gypsum in delaying the heat transfer and increasing the fire resistance of the system is the endothermic reaction of dehydration. As this reaction absorbs heat, it delays heat transfer through the system. Comparing the results of STA tests, we observe that the energy of this reaction in the type F gypsum plasterboard is approximately 3.6 % higher than that measured in the type N gypsum plasterboard. Although this result may explain an increase in benefits of this gypsum plasterboard it does not the full extent of the improvement obtained in systems with this type of gypsum plasterboard. The content of mineral fibre in the type F gypsum plasterboard core, which enhances its cohesion, should be the main cause of its better behaviour in fires.

After analysing the two kinds of boards, we performed a test on the cardboard used to cover the gypsum plasterboards. We studied its behaviour in air and in a nitrogen atmosphere. Therefore, we were able to analyse the cardboard behaviour in conditions that allow combustion or only pyrolysis. In real situations, cardboard is present at the interface between boards without sufficient oxygen to burn and in the exposed side of the boards with sufficient oxygen to burn.

We performed an STA test for the cardboard used to cover the type F gypsum plasterboard. The test was developed at a heat rate of  $10 \text{ K}\cdot\text{min}^{-1}$  in a nitrogen atmosphere (Figure 3). This nitrogen-atmosphere analysis is of great interest as the availability of oxygen between two plasterboards is limited, and thus combustion cannot occur. Similar results to previous TG studies have been obtained for cardboards [16, 17]. Changing only the atmosphere from nitrogen to air, we performed the same test with the same material (Figure 4).

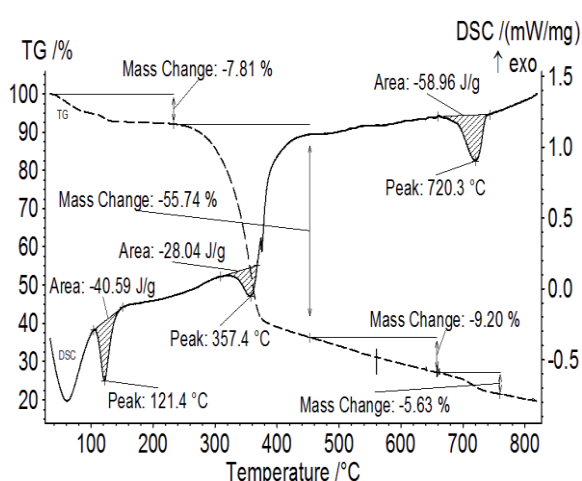


Fig. 3. DSC (solid line) and TG (dashed line) results for cardboard in  $\text{N}_2$  atmosphere.

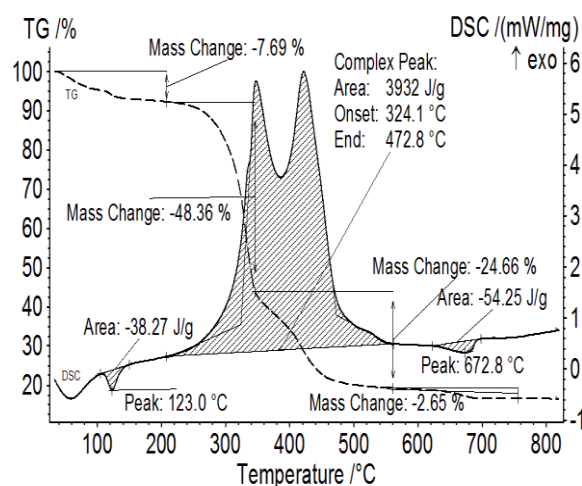


Fig. 4. DSC (solid line) and TG (dashed line) results for cardboard in air.

The initial cardboard mass of the tested samples were 10.675 mg for the nitrogen test and 11.190 mg for the air test. An initial mass loss of 7.81 % in  $\text{N}_2$  and 7.69 % in air conditions occurs in both tests between 30 and 200 °C. The energy absorbed in both cases was so similar. This first mass loss is related to the moisture content loss [18]. Above 200 °C, the behaviour under both atmospheres differed according to the energy released or absorbed. DSC shows the energy released or absorbed per unit of mass. For the test in air, we clearly distinguished two exothermic reactions with a total heat release of approximately  $3932 \text{ J}\cdot\text{g}^{-1}$ . The two reactions were consecutive and corresponded to the main mass loss of the sample. These reactions occurred between 205 and 560 °C (Figure 4). For the  $\text{N}_2$  atmosphere, endothermic reactions, in which absorb  $28.04 \text{ J}\cdot\text{g}^{-1}$ , took place between 225 and 450 °C (Figure 3). This endothermic reaction could include the hemicellulose decomposition, which was established between 250 and 350 °C, and the cellulose decomposition that appeared between 325 and 400 °C [19]. The total mass loss in air was 83.36 %, close to the 78.38 % for mass loss in  $\text{N}_2$  (Tables 4 and 5).

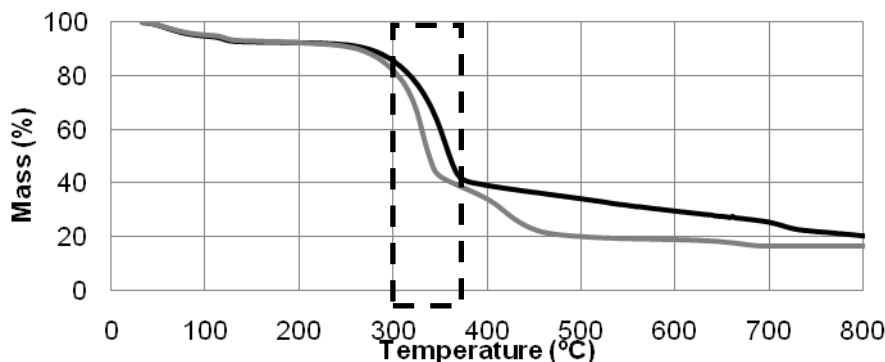


Fig. 5. Comparison of TG results for cardboard in air (grey) and  $\text{N}_2$  (black).

As shown in Figure 5, most of the mass loss of cardboard took place at the same temperatures in N<sub>2</sub> and air atmosphere. This loss was approximately 60 % of the initial mass at approximately 300 and 375 °C, which corresponded to the temperatures at which exothermic reactions occurred in the gypsum, in which the molecular structure of the soluble crystal reorganizes itself into a lower insoluble energy state [5]. [20] shows bending test results in which, it can be seen that failure load of type F and N gypsums plasterboards without cardboard decrease after dehydration, and then decrease more after the transition reaction. These tests showed that critical temperatures in gypsum and cardboard are between 300 and 375 °C. This range is valid for gypsum and for cardboard. The cardboard is the component that provides mechanical resistance against deflection and is supported by the difference in the flexural strength of gypsum plasterboard considering bearing edges perpendicular or parallel to length reported by manufacturers, and associated to the cardboard in our study and in the literature [21]. As a result, we considered the hypothesis that at this range of temperature, gypsum plasterboards would begin to fall.

### 3. STANDARD FIRE TESTS

Standard fire tests [2, 3, 4] were performed for the different configurations summarized in Table 6. The samples tested had an area of 3 x 3 m and the test furnace had to maintain the average temperatures at the values specified by the standards.

$$T = 345 \cdot \log_{10}(8t + 1) + 20 \quad (4)$$

To validate the thermal model of FDS in the simulation of gypsum plasterboard, we used standard fire tests results of three ceiling systems composed of boards without any cavities between them.

The first, second and third tests were composed of one 15 F, two 13 F and three 15 F plasterboards, respectively (Table 6). This selection allows to compare the behaviour of the system with the use of several parallel boards without air cavity, and to validate the model prediction of the thermal conductivity through the boards. Figure 6 shows the normalized failure temperature for the tests. To normalize, we subtract the ambient temperature from the measured values.

We observed in the curves of temperature the same heating steps in all the tests, but with some differences (Figure 6). The unexposed temperature increases until the dehydration process happened in the gypsum plasterboards, which was represented in the unexposed curves by a constant temperature and was caused by the absorption of heat that this process required, which prevented a temperature increase. Systems with more than one board had different steps of constant temperature due to dehydration of the different boards. When the dehydration process is finished, we observe an increase in the temperature, followed by a sharp increase in temperature at failure of the system.

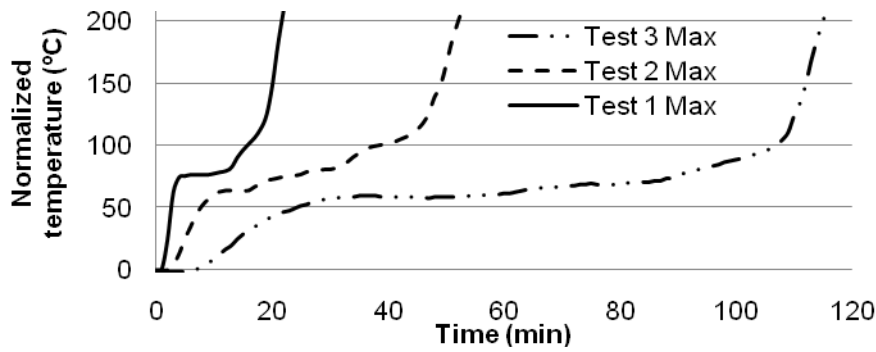


Fig. 6. Normalized temperatures on the unexposed face during tests 1, 2 and 3.

In addition, tests 4, 5 and 6 allowed to validate the model against different sort of gypsum plasterboard systems, with and without mineral wool in the cavity (Table 6).

The system of test 4 was composed of two 13 N boards attached to a stud of 0.5 mm thick galvanized steel and another two 13 N boards on the other side. Gypsum plasterboards had a thickness of 13 mm. The system was filled with mineral wool with a thickness of 45 mm. The mineral wool employed had a thermal conductivity of  $0.04 \text{ W}\cdot\text{m}^{-1}\cdot\text{K}^{-1}$ , a density in the range of  $15 \text{ to } 20 \text{ kg}\cdot\text{m}^{-3}$  and a specific heat of  $0.8 \text{ kJ}\cdot\text{kg}^{-1}\cdot\text{K}^{-1}$ .

The positions of the strain gauges and thermocouples are shown in Figure 7 and Table 7. Strain gauges, installed on the unexposed surfaces and perpendicular to the gypsum plasterboards, allowed us to measure the deformation of the system at different points and, thus, to study qualitatively how deformation relates to the collapse of the system. The most relevant board temperatures were taken from the three positions shown in Figure 7: on the unexposed face (Tc28, Tc29 and Tc30), at the interior face of the unexposed boards (Tc45, Tc47 and Tc49), and at the interior face of the exposed boards (Tc44, Tc46 and Tc48). Thermocouples, numbered from 1 to 27, were positioned in the metal stud. The furnace had some little windows from where the behaviour of the exposed face was observed.



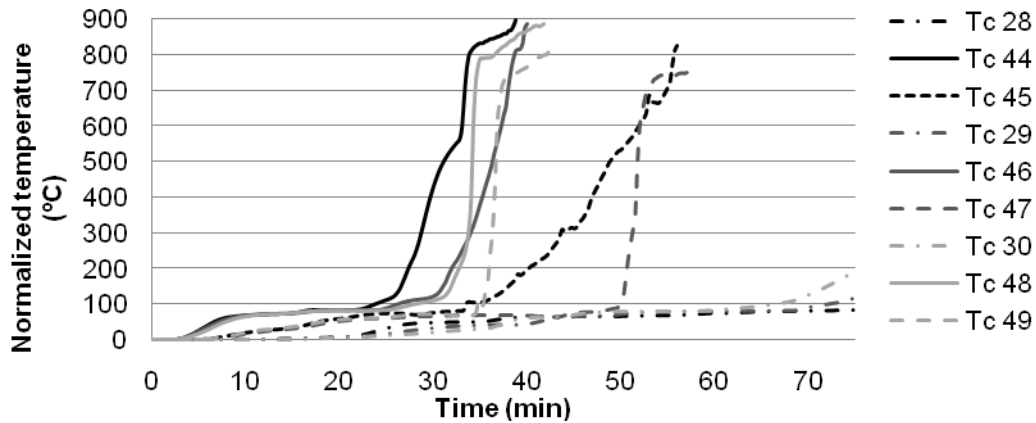


Fig. 8. Temperature vs. time at the interior face of the system during test 4.

A summary of the results is shown in Table 8. This table indicates the key points, which are defined by the trend change of the temperature curves. There are very close results of the temperature and time values for the different process. As expected, thermocouples closer to the furnace showed a temperature increase up to 100 °C in the first stage and then remained at this temperature while the exposed gypsum board lost its moisture content. Afterward, when the exposed board was dehydrated, there was an increase of approximately 30 °C in the temperature on the interior of the exposed boards since more heat passed through the first dehydrated board, and more dehydration took place in the second of the exposed boards. This happened between the minutes 22 to 25.75 for Tc44, the minutes 24.5 and 30 for Tc46, and the minutes 25 and 30.5 for the Tc48, respectively. When both exposed and unexposed boards were dehydrated, more heat was transferred by radiation through the system having the temperature an exponential increase.

Figures 9 and 10 show the axial deformation of the more relevant points and the temperatures in the stud for each of these positions.

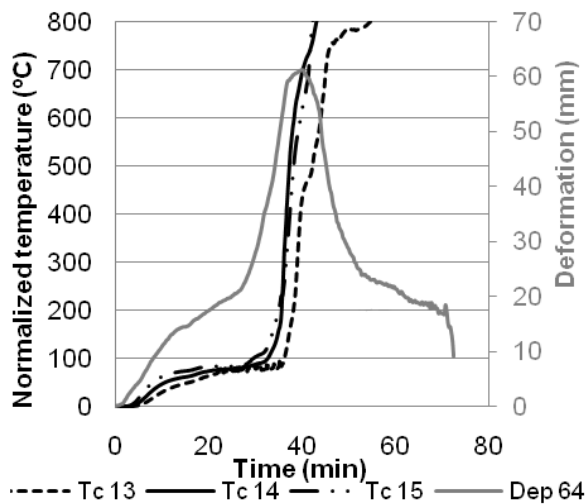


Fig. 9. Axial deformation and stud temperature at measure point 64 during test 4.

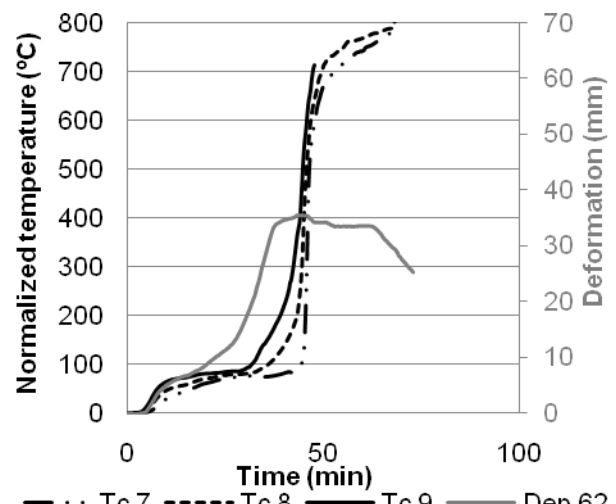


Fig. 10. Axial deformation and stud temperature at measure point 62 during test 4.

It can be seen from Figures 9 and 10 that, after a steady stage at a temperature of approximately 100°C, the deformation of the stud became to increase more rapidly when the temperature of the studs grew sharply. This is directly related to the conduction of heat that

happened between the inner exposed board and the studs. The heat transferred rapidly to the stud owing to its high thermal conductivity. As the measured point 64 was closer to the middle of the system, more deformation was observed, 60.8 versus 34.7 mm in the measure point 62.

Figure 11 displays the temperatures on the unexposed face at the locations where failure temperature was reached first. Thermocouple Tc30 reached 180°C above ambient temperature (condition for failure) at 74.5 min. This thermocouple was positioned in the centre of the system.

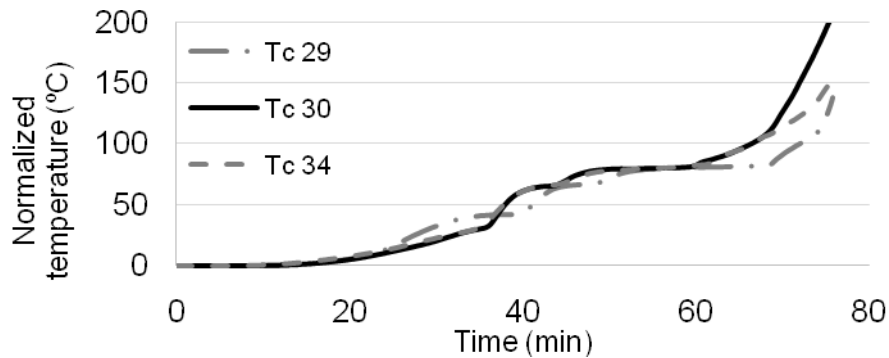


Fig. 11. Normalized temperatures on the unexposed face during test 4.

The system for test 5 was composed of a steel H-stud of 48 mm depth and a separation between the studs of 600 mm. On each side of the stud, there were two F plasterboards. The stud provided an air gap in the system. The positions of the strain gauges and thermocouples are listed in Figure 7.

Figures 12 and 13 show the normalized temperatures in the interior and at three points on the unexposed face of the system. Figure 13 depicts the temperature of the unexposed face that reaches the failure temperature first. Thermocouples close to the furnace indicated temperatures in the range of 80 to 100 °C between 10 and 28.5 min. After that, the temperature increased up to 130 °C at minute 43, and then began to grow sharply (Tc44, Tc46 and Tc48).

This test 5 differs from the previous one in the behaviour of the temperatures on both sides of the air gap. Table 9 summarizes the results of test 5. We observed a constant temperature of approximately 92.8 to 100 °C in the interior surface of the unexposed plasterboards until a sharp increase took place. Thermocouples in the unexposed board had a weak but constant increment in temperature up to 100 °C at minute 135.4 (Table 9), followed by a sharp raise that caused the system to fail. Thermocouple Tc 34 reached 180°C above the ambient temperature at 150 min.

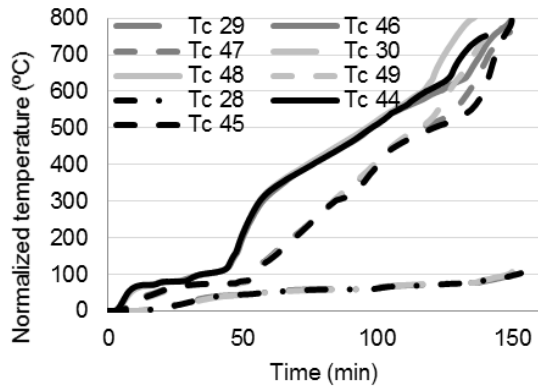


Fig. 12. Normalized temperatures vs. time at the interior face of the system during test 5.

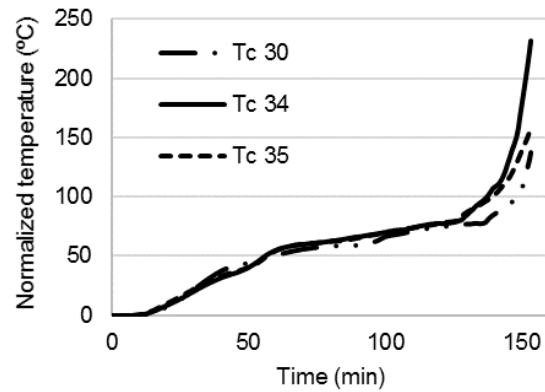


Fig. 13. Normalized temperatures on the unexposed face during test 5.

Figures 14 to 22 present the deflection and temperatures in the studs at the measuring points 60 to 68. As in the test 4, the stud deflection increased at all points because of the temperature increase in the studs. This stud temperature increase is due to the temperature spread in the exposed plasterboard. We observed the first step of constant temperature caused by gypsum dehydration and, after this first step, the temperature and the stud deflection began to increase.

This behaviour could be seen in all the measure points. The maximum axial deflections were measured along the  $\Omega$  axis since it is closer to the middle of the system. As the measure points along the axis  $\varphi$  are closer to the side of the furnace, there were more restriction to deflect, and lower values were registered. Deflection behaviour measured along  $\pi$  and  $\Omega$  axis was mostly the same.

The maximum axial deflection was approximately 100 mm, and it was obtained in the gauge 64, which is the closer measure point to the middle of the system.

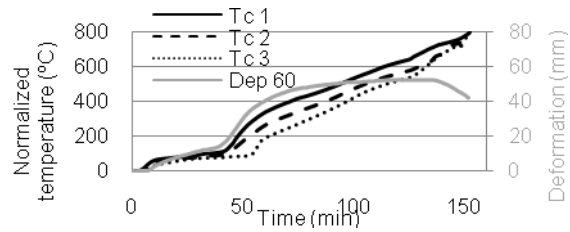


Fig. 14. Axial deformation and stud temperature at measure point 60 in test 5.

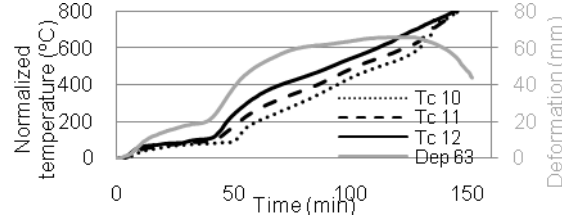


Fig. 15. Axial deformation and stud temperature at measure point 63 in test 5.

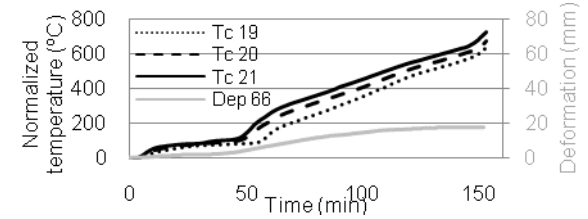


Fig. 16. Axial deformation and stud temperature at measure point 66 in test 5.

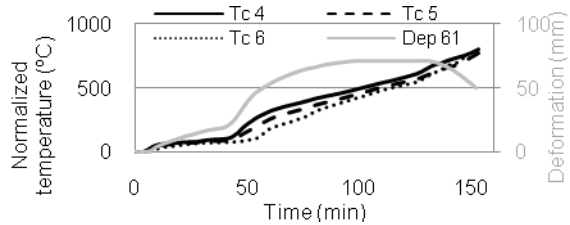


Fig. 17. Axial deformation and stud temperature at measure point 61 in test 5.

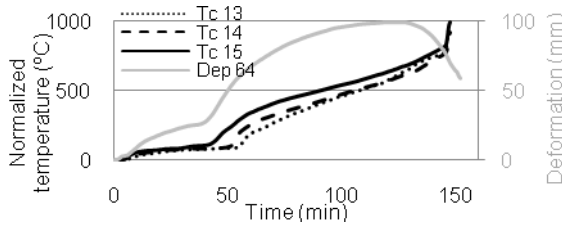


Fig. 18. Axial deformation and stud temperature at measure point 64 in test 5.

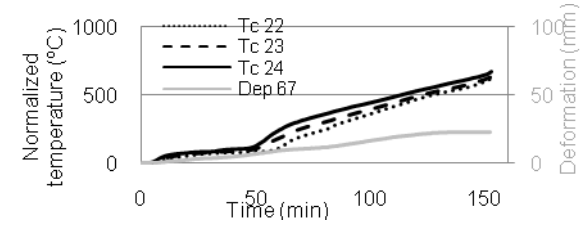


Fig. 19. Axial deformation and stud temperature at measure point 67 in test 5.

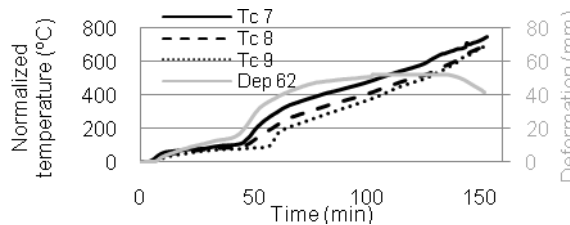


Fig. 20. Axial deformation and stud temperature at measure point 62 in test 5.

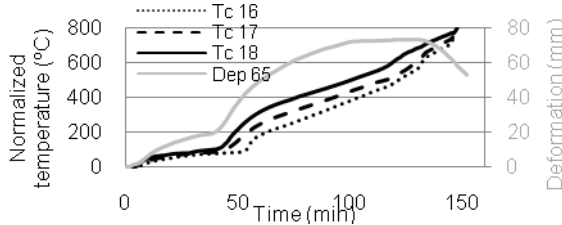


Fig. 21. Axial deformation and stud temperature at measure point 65 in test 5.

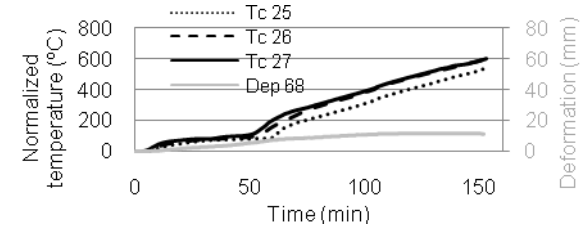


Fig. 22. Axial deformation and stud temperature at measure point 68 in test 5.

Figures 23 and 24 display the axial deflection along the width and height of the system at the moment of maximum axial deflection (124 min). The distribution of the deflection lines  $\alpha$ ,  $\beta$ ,  $\mu$ ,  $\pi$ ,  $\Omega$  and  $\phi$  in the system are represented in Figure 7. The points plotted in Figure 23 show the joints between the different unexposed boards, and thus the absolute deflection for each board is that between the deflection curve and the imaginary straight line that links the points. Taking into consideration the internal boards that range from 0 to 1200 mm (straight line in the figure), 1200 mm to 2400 mm, and from 2400 to 3000 mm, one finds the maximum horizontal deflection is approximately 25 mm, as shown in Figure 23 (straight dashed line).

Figure 24 includes the axial deflection along the vertical lines ( $\alpha$ ,  $\beta$  and  $\mu$ ). The first 3 m correspond to one board, and the rest corresponds to a different board. The maximum deflection in the 3 m high board is approximately 80 mm, as shown in the straight dashed line in Figure 24. These plasterboard systems were highly flexible, provided the cardboard was not degraded. When the cardboard got thermally degraded, the system begins to collapse, and board pieces fall out.

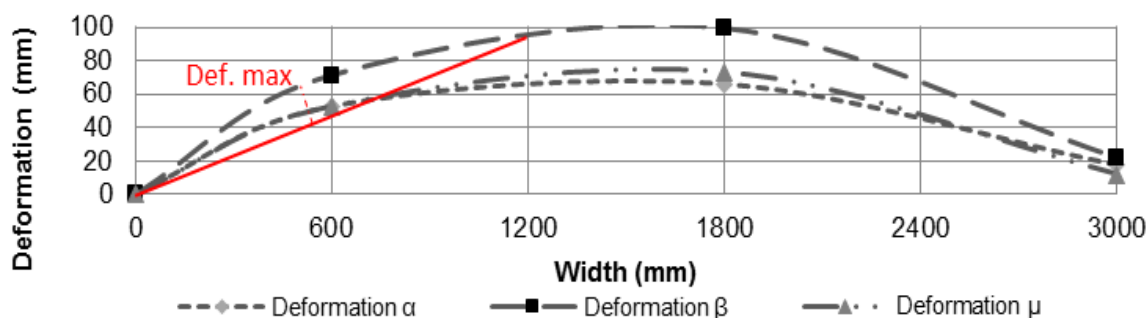


Fig. 23. Axial deflection of boards in horizontal direction in test 5.

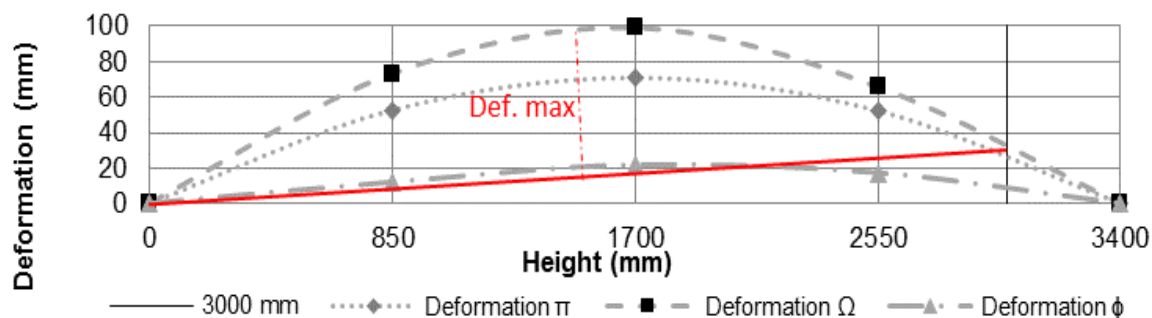


Fig. 24. Axial deflection of boards in vertical direction in test 5.

Test 6 was composed of a system with a steel stud of 46 mm depth and a separation between the studs of 600 mm. On each side of the stud, there were 18 N gypsum plasterboards. The studs provided air gaps in the system. The positions of the thermocouples are listed in Figure 7. Figure 25 shows the temperatures in the interior and in the unexposed face of the system during test 6 for the two most critical positions. Failure of the system took place at minute 69 in Tc30 and at minute 71 in Tc36. These measuring points were located at the centre of the system, separated by 30 cm. Tc13 and Tc15 corresponded to the metal profile stud.

Although Tc36, Tc13 and Tc15 coincided to the thermal bridge, no remarkable differences were found in the unexposed temperatures. However, in Figure 25 we can see that Tc48 and

Tc15 had such a similar temperature profile until minute 23, when both temperatures began to increase. We observed the thermal bridge effect in the temperature of the metal stud, which allowed Tc13 to rise its temperature earlier due to thermal conductivity through the stud. Figure 26 shows the normalized temperature curves in the unexposed face. Failure of the system was reached at minute 69.

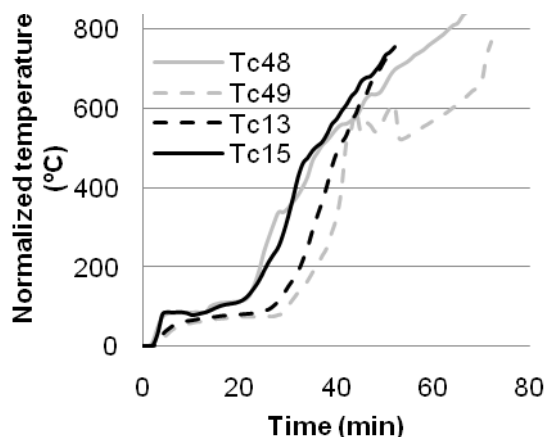


Fig. 25. Normalized temperatures vs. time at the interior face of the system during test 6

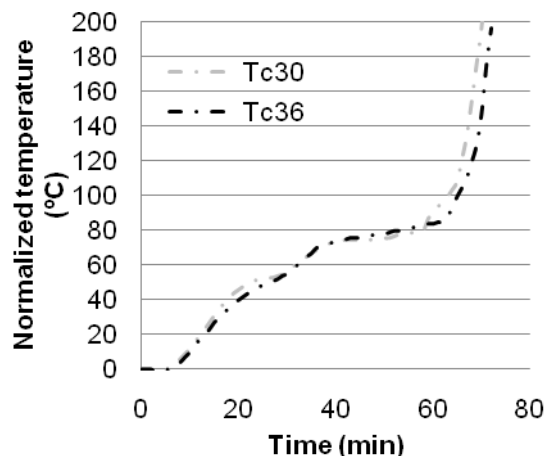


Fig. 26. Normalized temperatures vs. time in the unexposed face of the system during test 6

#### 4. THERMAL MODEL

The numerical model developed employs the Fire Dynamics Simulator (FDS) [22, 23]. The main factor that provides more resistance to bending of the plasterboard was the cardboard [21]. Therefore, when the cardboard was thermally degraded, weak strain could cause board pieces to fall out. The temperature of thermal degradation of the cardboard was investigated in this study and had a peak value of approximately 347 and 360 °C for air and nitrogen, respectively. In addition, at approximately this range of temperature, the gypsum undergoes a transition reaction to an anhydride state. Following this reaction, the gypsum becomes weaker. Based on this hypothesis, as the cardboard was the one that had the higher flexural resistance in the gypsum plasterboards, our model did not have to consider the gypsum cracking, because when the cardboard was thermally degraded, the gypsum would not offer any resistance to flexural efforts.

The dehydration reactions of F and N plasterboards studied by STA measurements were incorporated in the model by the mass loss and energy absorbed in the process. The model considered a gypsum plasterboard sample of  $50 \times 50 \text{ mm}^2$ , with a mesh size of 5 mm for the gas zone and 2.5 mm for solids, as we assumed homogeneous behaviour of heat transfer through the whole system without consider steel stud. The 2.5 mm size employed in the model was the mean size of the dedicated computational mesh used by FDS to solve the 1D heat conduction equation in the solid phase. This value is possible because the solid regions obey the ‘one cell thick’ rule of FDS and it allows a better resolution of the heat conduction through the plasterboards. We used  $\text{CELL\_SIZE\_FACTOR} = 0.5$  to decrease the mesh size from 5 to 2.5 mm, and the  $\text{STRETCH\_FACTOR} = 1$  to generate a perfectly uniform mesh in the solid. When one applies boundary conditions to the backside, the model uses the attribute  $\text{BACKING} = \text{‘EXPOSED’}$  and is required to calculate the heat transfer through the solid into the space behind the solid. Side of the plasterboards were thermally insulated in order to allow only heat losses through the axial direction. The wall emissivity of all gypsum plasterboards

was assumed to be 0.88 [24]. Density, thermal conductivity and specified heat of F and N plasterboards were obtained from reference [15]. Thermal conductivity and specific heat were thermally dependent. While values of densities are 691 and 777  $\text{kg}\cdot\text{m}^{-3}$  for N and F plasterboards at ambient temperature respectively, thermal conductivity and specific heat at ambient temperature were 0.0793 and 0.147  $\text{W}\cdot\text{m}^{-1}\cdot\text{K}^{-1}$ ; and 0.4289 and 0.704  $\text{J}\cdot\text{g}^{-1}\cdot\text{K}^{-1}$  for N and F plasterboards at ambient temperature, respectively. The kinetics parameters, activation energy (A) and pre-exponential factor (E), are not available for most real materials. FDS can estimate them from a TG experimental test [22]. We used the experimental tests results of the dehydration peak temperature, heating rate and pyrolysis range for both gypsum plasterboards to define the kinetic parameters in the FDS model.

The plasterboard model was divided into obstructions of 1  $\text{cm}^2$  in area. Each of these obstructions had an associated device to measure its unexposed temperature. With this temperature and using an FDS control function (&CTRL), the model made the obstruction disappear at the considered falling out temperature so as to simulate plasterboard fall out in the FDS model. The cells of the disappeared obstructions were filled with air.

For tests 1, 2 and 3, the hypothesis that considered the falling out of the boards was not relevant, as the failure of the systems happened before the gypsum plasterboards reached the temperature required to fall. Figure 27 shows the validation of the model for tests 1, 2, and 3. The grey and black curves represent the simulated and experimental normalized temperature, respectively. As shown, the thermal model of FDS provided a good agreement between tests and simulations. Test 1 obtained a normalized temperature of 180 °C at the minute 21 for the experimental test, and at the minute 23 for the simulation. Test 2 indicated a normalized temperature of 180 °C at the minute 51 for the experimental test, and at the minute 51.8 for the simulation. Finally, test 3 showed a normalized temperature of 180°C at the minute 114 for the experimental test, and at the minute 112.8 for the simulation.

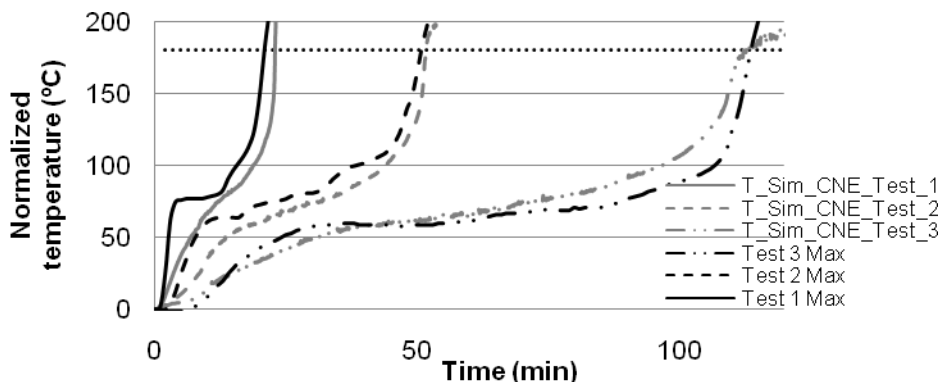


Fig. 27. Comparison of simulated and experimental temperatures in the unexposed face in tests 1, 2 and 3.

Applying the developed model to the system tested in test 4, we obtained the temperature curves depicted in Figs. 28 and 29. These curves show the temperatures at two locations at the interior face of the system, in the zone of the exposed board and the unexposed board. We can see that the simulated temperature profile of the interior face of the exposed boards (continuous) had a shape similar to that of the experimental profiles (dashed lines). The sharp increase in temperature caused by the dehydration of the gypsum in the model had a delay of approximately 7 min.

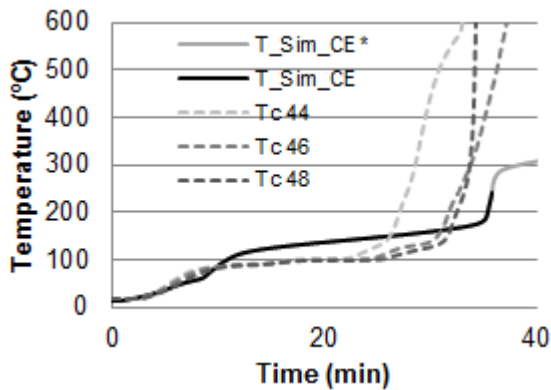


Fig. 28. Comparison of simulated and experimental temperatures at the interior face of the exposed board in test 4.

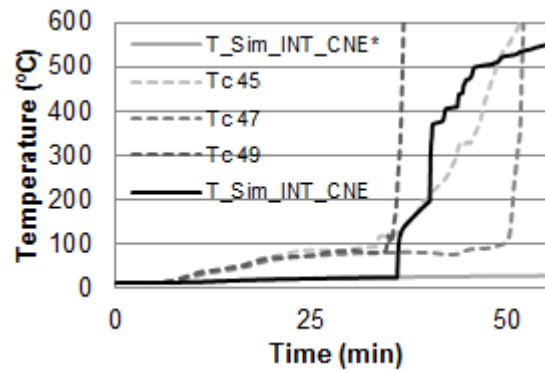


Fig. 29. Comparison of simulated and experimental temperatures at the interior face of the unexposed board in test 4.

The temperature on the internal face of the unexposed board is shown in Figure 29. The initial simulated temperature was close to ambient temperature because of the limitation of FDS on the study of heat transfer by conduction through several obstructions. If the obstruction is more than one cell thick, it is assumed to back up to an air gap at ambient temperature. However, as our model predicted the falling out of the boards, which permitted the flux of hot gas to pass to the unexposed boards, we obtained a good approximation of the moment at which the temperature raise at the interior face of the unexposed board. This also provided a good approximation of the unexposed temperature (failure temperature).

Figure 30 is a comparison of the experimental and simulated temperature curves of the unexposed face in test 4, and it partially validates the model. Although we initially obtained a very low increase in temperature, after the boards fall out the simulated unexposed temperature agreed well with the experimental one, and the model calculated a failure time of 75 min, which closely approximates the experimental failure time of 74 min. As we can see in the FDS predictions where no “fall-off” model had been used (grey continuous line), there was not a good agreement with the temperatures results since it only considered the insulation of the system at the initials conditions, without taking into account the degradation effect of the heat flux in the studied system.

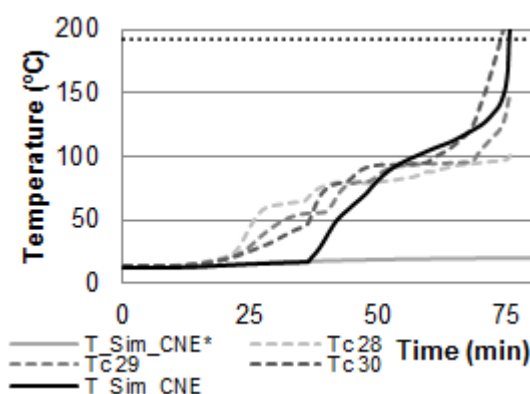


Fig. 30. Comparison of simulated and experimental temperatures at the unexposed face in test 4.

Figure 31 shows the simulated and experimental temperatures at the interior face of the system for test 5. Good agreement was obtained for the first 44 min that corresponded to the gypsum dehydration process.

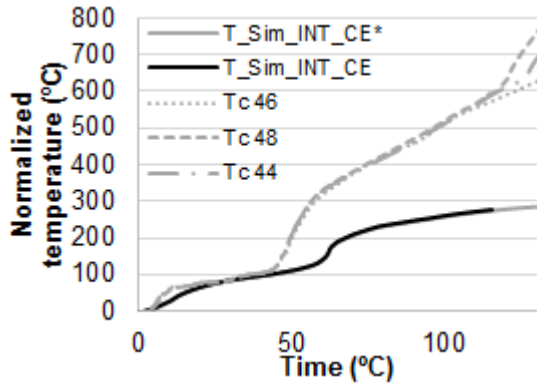


Fig. 31 Comparison of simulated and experimental temperatures at the interior face of the exposed board in test 5.

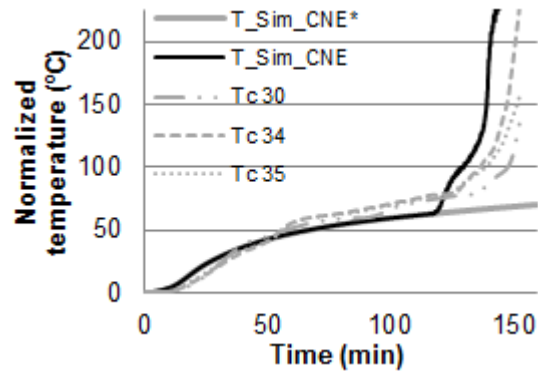


Fig. 32 Comparison of simulated and experimental temperatures in the unexposed face in test 5.

Comparing test results for the unexposed face (Figure 32) with the simulation, we observed good agreement in the temperature curves. At approximately 120 min, a sharp increase in the simulated temperature initiates. This meant that the dehydration process was near completion. This happened at 124 min in the experimental test. Failure in the simulated test occurred at 140 min, 10 min earlier than in the experimental test. This is an error of 6.6 %. Result of the model without “fall-off” of the plasterboards (grey continuous line) shows that, although the temperature had slightly increased in the unexposed side, not enough heat was reaches to complete dehydration in the unexposed boards.

Finally, Figs. 33 and 34 show the validation for test 6. Figure 33 displays the normalized temperatures at the interior face of the unexposed face. It is provided a good agreement in the results until minute 30. Then, the experimental temperature grew more rapidly than the simulated temperature. The simulated temperature curve at the unexposed face correlated well with the experimental results. Experimental failure took place at minute 69, whereas simulated failure at minute 72.9 (error of 5.6 %). As in the test 5 predictions of the model without considering “fall-off” (grey continuous line), no failure was reached in that case.

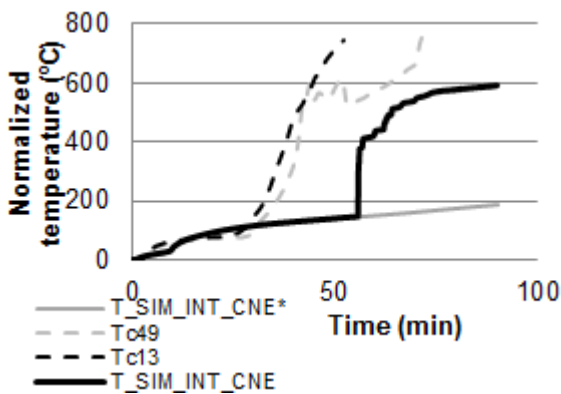


Fig. 33. Comparison of simulated and experimental temperatures at the interior of the unexposed board in test 6.

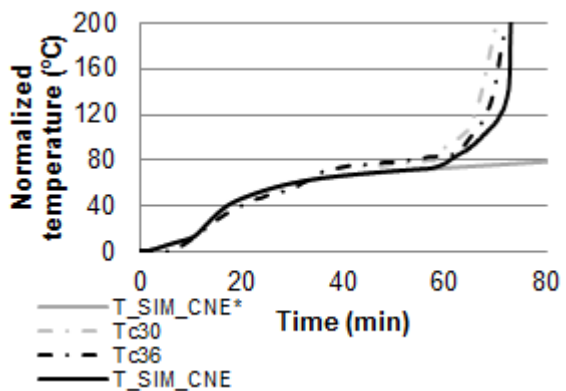


Fig. 34. Comparison of simulated and experimental temperatures in the unexposed face in test 6.

## 5. CONCLUSIONS

This study investigated the effect of the cardboard in the fire resistance of gypsum plasterboard systems, in order to model the failure of the gypsum plasterboards systems under

full-scale fire resistance tests. This paper has presented a gypsum plasterboards systems failure model based on cardboard behaviour, based on thermogravimetric analyses of different kinds of gypsums and cardboards have been performed. Comparison between the degradation of the cardboard under different atmospheres was also studied to define the applicability of the failure hypothesis.

Six full-scale fire resistance tests were analysed so as to obtain a better understanding of the processes that are involved in the failure of the systems, and also to validate the failure model. This failure model was developed in FDS, including the gypsum dehydration effect in the heat transfer through the system. In addition, it was considered the hypothesis of the fall off the gypsum plasterboards.

Good agreement in the model result was obtained with the hypothesis developed in the present work. This hypothesis considered the degradation of the cardboard to be the critical point at which plasterboard loses most of its resistance. This took place at temperatures of approximately 347 and 360°C for air and the nitrogen atmosphere, respectively. The study of the nitrogen atmosphere was relevant because of the lack of air in the layer between the plasterboards, or between plasterboards and the insulation.

While processes in types N and F gypsum plasterboards were the same, there were some differences in the TG and DSC curves. The corresponding processes in the two gypsum plasterboards occurred at similar temperatures.

Our experimental results showed the relation between the heat transfer through the system and the deflection. When the normalized stud temperature exceeded 100°C, it could be seen that the deflection in the unexposed face begins to increase significantly. This temperature increase means that exposed gypsum plasterboards were completely dehydrated and could not absorb more heat. This means that although mechanical forces affect the system, they were a consequence of the gypsum dehydration, so the heat transfer is the main factor in the fire resistance of building systems.

Results of the present study are useful not only for modelling, but also for plasterboard manufacturers. A treatment to improve fire resistance of cardboard will provide an enhancement in the fire resistance of gypsum plasterboard systems.

## Acknowledgments

The authors would like to thank the Spanish Ministry of Economy and Competitiveness for the PYRODESIGN Project grant, Ref.: BIA2012-37890, financed jointly by FEDER funds.

This is a pre-print of an article published in *Fire & Materials*. The final authenticated version is available online at: <https://onlinelibrary.wiley.com/doi/epdf/10.1002/fam.2483>

## References

- [1] Stec, A. A., Hull, T R., Assessment of the fire toxicity of building insulation materials, *Energy and Buildings*, 43 (2-3), pp. 498-506 (2011) doi:10.1016/j.enbuild.2010.10.015
- [2] UNE-EN 1363-1: Fire resistance tests. Part 1: general requirements. 2000.
- [3] UNE-EN 1364-1:2000. Fire resistance tests for non-load bearing elements. Part 1: walls. 2000.
- [4] UNE-EN 1364-2: Fire resistance tests for non-loadbearing elements—Part 2: ceilings. 2000.

- [5] Manzello SL, Gann RG, Kukuck SR, Lenhert DB. Influence of gypsum board type (X or C) on real fire performance of partition assemblies. *Fire and Materials* 2007; 31:425–442.
- [6] Hopkin, D. J., Lennon, T., El-Rimawi, J., Silberschmidt, V. V., A numerical study of gypsum plasterboard behaviour under standard and natural fire conditions, *Fire and Materials* 2012; 36:107–126.
- [7] Mehaffey JR, Cuerrier P, Carisse GA. A model for predicting heat transfer through gypsum-board/wood-stud walls exposed to fire. *Fire and Materials* 1994; 18:297–305.
- [8] Kolaitis DI, Founti MA. Development of a solid reaction kinetics gypsum dehydration model appropriate for CFD simulation of gypsum plasterboard wall assemblies exposed to fire. *Fire Safety Journal* 2013; 58:151–159.
- [9] Manie, J., Kikstra, W. P., DIANA - Finite Element Analysis User's Manual release 9.6, TNO Building and Construction Research: Delft, The Netherlands, 2015
- [10] P. Keerthan, M. Mahendran, Numerical studies of gypsum plasterboard panels under standard fire conditions, *Fire Safety Journal*, Volume 53, October 2012, Pages 105–119
- [11] J.M. Franssen. T. Gernay, User's manual for SAFIR 2016c a computer program for analysis of structures subjected to fire, University of Liege, Institute Du Genie Civil, Liege, Belgium
- [12] I. D. Thanasoulas, I. K. Vardakoulis, D. I. Kolaitis, C. J. Gantes, M. A. Founti, Thermal and Mechanical Computational Study of Load-Bearing Cold-Formed Steel Drywall Systems Exposed to Fire, *Fire Technology*, Volume 52, Issue 6, pp 2071–2092, 2016
- [13] ANSYS 15.0 (2013) User's Guide ANSYS Inc. Canonsburg
- [14] ADINA System 8.5 (2008) Release Notes ADINA R&D Inc. Watertown
- [15] Lázaro, D., Puente, E., Lázaro, M., Lázaro, P. G., Peña J., Thermal modelling of gypsum plasterboard assemblies exposed to standard fire tests. *Fire and materials*, 2016; 40:568–585.
- [16] McKinnon, M. B., Stoliarov, S. I., Witkowski, A., Development of a pyrolysis model for corrugated cardboard, *Combustion and Flame* 2013; 160: 2595–2607.
- [17] Agarwal, G., Liu, G., Lattimer, B., Pyrolysis and Oxidation of Cardboard, *Fire safety science-draft proceedings of the eleventh international symposium, IAFSS*, 2014.
- [18] David, C., Salvador, S., Dirion, J.L., Quintard, M., Determination of a reaction scheme for cardboard thermal degradation using thermal gravimetric analysis., *Journal of Analytical and Applied Pyrolysis* , 2003; 67(2): 307-323.
- [19] Ghorbel, L., Rouissi, T., Brar, S.K., López-González, D., Ramirez, A.A., Godbout, S., Value-added performance of processed cardboard and farm breeding compost by pyrolysis, *Waste Management*, 2015, 38: 164–173
- [20] Rahmanian, I., Thermal and mechanical properties of gypsum boards and their influences on fire resistance of gypsum board based systems, Thesis, University of Manchester, 2011
- [21] Cramer, S.M.; Friday, O.M.; White, R.H.; Sriprutkiat, G. 2003. Mechanical properties of gypsum board at elevated temperatures. *Fire and materials* 2003: 8th International Conference, January 2003, San Francisco, CA, USA. London : Interscience Communications Limited, 2003: pages 33-42
- [22] McGrattan, K., et al. Fire dynamics simulator user's guide. NIST special publication. 1019, Sixth Edition. 2015
- [23] McGrattan, K., et al. Fire dynamics simulator technical reference guide. NIST special publication. 1018-1, Sixth Edition. 2015.
- [24] Ozisik MN, Heat transfer: a basic approach. New York, London; McGraw-Hill; 1985



<b>Material</b>	<b>Atmosphere</b>	<b>Heat rate (K/min)</b>	<b>Holder</b>
Gypsum of type N gypsum plasterboard	Air	10	With lid
Gypsum of type F gypsum plasterboard	Air	10	With lid
Cardboard of type F gypsum plasterboard	N <sub>2</sub>	10	
Cardboard of type F gypsum plasterboard	Air	10	

Table 1. Tested materials and conditions.

<b>N° Reaction</b>	<b>Initial temp. (°C)</b>	<b>Final temp. (°C)</b>	<b>T<sub>peak DSC</sub> (°C)</b>	<b>Final mass (mg)</b>	<b>Heat of reaction(J/g)</b>	<b>Mass loss (%)</b>
1 and2	85	194	142	15.64	-464.40	16.30
3	194	503	360	15.62	26.53	0.09
4	503	567	539	15.53	-11.94	0.51
5	567	759	687	15.18	-42.56	1.84

Table 2. Summary of STA results for type N gypsum plasterboard.

<b>N° Reaction</b>	<b>Initial temp. (°C)</b>	<b>Final temp. (°C)</b>	<b>T<sub>peak DSC</sub> (°C)</b>	<b>Final mass (mg)</b>	<b>Heat of reaction(J/g)</b>	<b>Mass loss (%)</b>
1 and2	125.3	189.4	149.7	12.71	481.10	17.02
3	350.5	396.4	375.2	12.60	22.47	0.74
4	533.7	578.4	564.6	12.40	23.57	1.27
5	600	750	717.5	12.20	29.79	1.33

Table 3. Summary of STA results for type F gypsum plasterboard.

<b>N° Reaction</b>	<b>Initial temperature (°C)</b>	<b>Final Temperature (°C)</b>	<b>Final mass(mg)</b>	<b>Heat of reaction (J/g)</b>	<b>Mass loss (%)</b>
1		225	9.84	40.59	7.81
2	225	450	3.89	28.04	55.74
3	450	655	2.91	-	9.2
4	655	757	2.31	58.96	5.63

Table 4. Summary of STA results for cardboard in N<sub>2</sub> atmosphere.

<b>N° Reaction</b>	<b>Initial temp. (°C)</b>	<b>Final temp. (°C)</b>	<b>T<sub>peak DSC</sub> (°C)</b>	<b>Final mass(mg)</b>	<b>Heat of reaction (J/g)</b>	<b>Mass loss (%)</b>
1		205		10.33	38.27	7.69
2	205	348	348	4.88	3932	48.36
3	348	560	421.8	2.12		24.66
4	560	750		1.82	54.25	2.65

Table 5. Summary of STA results for cardboard in air.

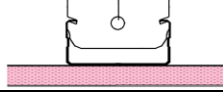
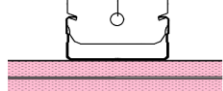
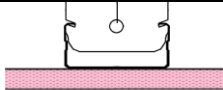
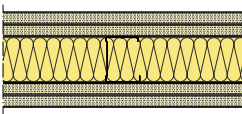
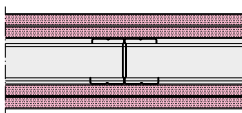
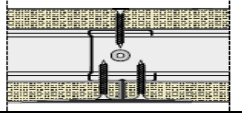
Test	Ambient temperature (°C)	System	Configuration	Insulation	Failure time (min)
1	10		F15	-	21
2	9		2x F13	-	51
3	15		3x F15	-	114
4	13		2x N13+ M48 +2x N13	Mineral wool	74
5	16		2x F13+ M48H +2x F13	Air	150
6	12		N18+ M46 + N18	Air	69

Table 6. Characteristics of fire resistance tests.

<b>Device</b>	<b>Width (mm)</b>	<b>Height (mm)</b>	<b>Deep (plane)</b>
Tc 1, 2, 3	618 / 600 / 618	2550	y / z / w
Tc 4, 5, 6	618 / 600 / 618	1700	y / z / w
Tc 7, 8, 9	618 / 600 / 618	850	y / z / w
Tc 10, 11, 12	1818 / 1800 / 1818	2550	y / z / w
Tc 13, 14, 15	1818 / 1800 / 1818	1700	y / z / w
Tc 16, 17, 18	1818 / 1800 / 1818	850	y / z / w
Tc 19, 20, 21	2982 / 3000 / 2982	2550	y / z / w
Tc 22, 23, 24	2982 / 3000 / 2982	1700	y / z / w
Tc 25, 26,27	2982 / 3000 / 2982	850	y / z / w
Tc 28, 44, 45	750	2550	x / w / y
Tc 29, 46, 47	2250	2550	x / w / y
Tc 30, 48, 49	1500	1500	x / w / y
SG 60, 61, 62	600	2550 / 1700 / 850	x
SG 63, 64, 65	1800	2550 / 1700 / 850	x
SG 66, 67, 68	3000	2550 / 1700 / 850	x

Table 7. Locations of strain gauges (SG) and thermocouples.

<b>Tc 44</b>		<b>Tc 46</b>		<b>Tc 48</b>	
Time (min)	Temperature (°C)	Time (min)	Temperature (°C)	Time (min)	Temperature (°C)
8	73.1	8	73.1	10	80.1
22	99.5	24.5	99.8	25	97.7
25.75	135.7	30	136.5	30.5	128.5
<b>Tc 45</b>		<b>Tc 47</b>		<b>Tc 49</b>	
Time (min)	Temperature (°C)	Time (min)	Temperature (°C)	Time (min)	Temperature (°C)
32.5	95.3	49	100.8	34	82.1
<b>Tc 28</b>		<b>Tc 29</b>		<b>Tc 30</b>	
Time (min)	Temperature (°C)	Time (min)	Temperature (°C)	Time (min)	Temperature (°C)
35.5	65.5	39.5	57.6	36	47.7
41.75	81.1	47.25	81.9	44.5	83.7
		67.25	96.7	59	96.4

Table 8. Summary of the results of Figure 8.

<b>Tc 44 - Tc 46 - Tc 48</b>		<b>Tc 45 - Tc 47 - Tc 49</b>		<b>Tc 28 - Tc29 - Tc 30</b>	
Time (min)	Temperature (°C)	Time (min)	Temperature (°C)	Time (min)	Temperature (°C)
16.5	90.3	47.5	92.8	50	62.2
28.5	101.2	52	100	95	78
43	129.9			135.4	95.3

Table 9. Summary of the results of Figures 12 and 13.